

Document downloaded from:

<http://hdl.handle.net/10251/67776>

This paper must be cited as:

Seguí-Simarro, JM.; Corral Martínez, P.; Corredor, E.; Raska, I.; Testillano, PS.; Risueno, M. (2011). A change of developmental program induces the remodeling of the interchromatin domain during microspore embryogenesis in *Brassica napus* L. *Journal of Plant Physiology*. 168(8):746-757. doi:10.1016/j.jplph.2010.10.014.



The final publication is available at

<http://dx.doi.org/10.1016/j.jplph.2010.10.014>

Copyright Elsevier

Additional Information

1
2
3
4 1 **A change of developmental program induces the remodeling of the interchromatin**
5
6 2 **domain during microspore embryogenesis in *Brassica napus* L.**
7
8
9 3

10
11 4 J.M. Seguí-Simarro¹, P. Corral-Martínez^{1,†}, E. Corredor^{2,†}, I. Raska³,
12
13 P.S. Testillano² and M.C. Risueño^{2,*}
14
15
16 6

17
18 7 ¹ Instituto para la Conservación y Mejora de la Agrodiversidad Valenciana (COMAV).

19 8 Universidad Politécnica de Valencia. Ciudad Politécnica de la Innovación (CPI). Edificio
20
21 9 8E - Escalera I. Camino de vera, s/n. 46022 Valencia. Spain.

22
23 10 ² Plant Development and Nuclear Organization. Centro de Investigaciones Biológicas
24
25 11 (CIB)-C.S.I.C. c/ Ramiro de Maeztu, 9. 28040 Madrid, Spain.

26
27 12 ³ Institute of Cellular Biology and Pathology, First Faculty of Medicine, Charles University
28
29 13 in Prague and Dept. of Cell Biology, Inst. of Physiology, Academy of Sciences of the
30
31 14 Czech Republic, v.v.i.,Albertov 4, 128 00 Prague, Czech Republic.
32
33
34
35
36
37
38
39
40

41 16 [†] These authors have contributed equally.
42
43
44

45 18 * Corresponding author. e-mail: risueno@cib.csic.es
46
47
48
49

50 20 Keywords: Cajal bodies, differentiation, maturation, microspore embryogenesis, nucleus,
51
52 21 pollen, proliferation, rapeseed.
53
54
55
56
57
58
59
60
61
62
63
64
65

1
2
3
4 **Abstract**
5
6
7
8

9 After a stress treatment, the in vitro-cultured pollen changes its normal
10 gametophytic developmental pathway towards embryogenesis producing multicellular
11 embryos from which, finally, haploid and double haploid plants develop. The architecture
12 of the well-organized nuclear functional domains changes in response to DNA replication,
13 RNA transcription, processing and transport dynamics. A number of subnuclear structures
14 present in the interchromatin region (IR, the nuclear domain between chromosome
15 territories) have been shown as involved, either directly or indirectly, in transcriptional
16 regulation. These structures include the interchromatin granule clusters (IGCs),
17 perichromatin fibrils (PFs), Cajal bodies (CBs) and perichromatin granules (PGs). In this
18 work, we present a cytochemical, immunocytochemical, quantitative and morphometric
19 analysis at the light, confocal and electron microscopy levels to characterize the changes in
20 the functional architecture of the nuclear interchromatin domain during two developmental
21 programs followed by the microspore: differentiation to mature pollen grains
22 (transcriptionally inactive), and microspore embryogenesis involving proliferation in the
23 first stages (highly engaged in transcription). Our results revealed characteristic changes in
24 size, shape and distribution of the different interchromatin structures as a consequence of
the reprogramming of the microspore, allowing us to relate the remodeling of the
interchromatin domain to the variations in transcriptional activities during proliferation and
differentiation events and suggesting that RNA associated structures could be a regulatory
mechanism in the process. In addition, we document the presence of two structurally
different types of CBs, and of IGC and CB-associated regions, similar to those present in
animal cells, and not yet described in plants.

1 **Introduction**

2
3
4
5
6 2
7
8
9 3 The microspore or immature pollen grain normally follows the gametophytic
10
11 4 program and differentiates to form the mature pollen, a process that can also be reproduced
12
13 5 in vitro. Upon the application of a stress treatment it can be deviated towards a proliferation
14
15 6 process leading to embryogenesis and plant regeneration, the so-called microspore
16
17 7 embryogenesis (Seguí-Simarro and Nuez 2008), a process which represents an important
18
19 8 tool in plant breeding to obtain double-haploid plants. The entry into proliferation of
20
21 9 differentiating cells is a key event in plant development and in organogenic and
22
23 10 morphogenetic processes. Since the cell nucleus governs the cell activity, the know-how of
24
25 11 the dynamics of the nuclear domains during the activation of such processes will give new
26
27 12 insights into the mechanisms that regulate them. Pollen developmental programs represent
28
29 13 model systems to analyze the cellular changes which accompany the change of
30
31 14 developmental program and the switch to proliferation from plant differentiating cells.
32
33
34
35
36
37
38
39

40 16 The nucleus is the cell factory where DNA replication and RNA transcription and
41
42 17 processing take place. It is a highly dynamic compartment where different activities are
43
44 18 confined to specific domains whose structure is markedly dependent on their function
45
46 19 (Spector, 1993a). Nuclear chromatin is divided in chromosome territories, which
47
48 20 encompass (1) condensed chromatin (heterochromatin, transcriptionally inactive) and (2)
49
50 21 decondensed chromatin (euchromatin) where transcriptionally active genes are located
51
52 22 (Cremer and Cremer, 2001). These different levels of condensation, together with other
53
54 23 remodeling and epigenetic events, are considered as a first, pretranscriptional level of
55
56 24 regulation of gene expression (Jarillo et al., 2009). Indeed, rearrangements in the position
57
58
59
60
61
62
63
64
65

1
2
3
4
5
6
7
8
9
10
11
12
13
14
15
16
17
18
19
20
21
22
23
24
25
26
27
28
29
30
31
32
33
34
35
36
37
38
39
40
41
42
43
44
45
46
47
48
49
50
51
52
53
54
55
56
57
58
59
60
61
62
63
64
65

1 and condensation of chromosomes are known to play an important role in the establishment
2 of the different developmental expression patterns by exposing and allowing access of the
3 transcriptional machinery to specific gene sequences. From a molecular point of view, the
4 different regulatory steps of transcription and pre-mRNA processing in eukaryotes are well
5 known processes. There is a wealth of data on how they proceed and the different
6 molecular players involved. Indeed, *in vitro* transcription is possible for long, which has
7 boosted the emergence of a pleiade of molecular biology techniques. However, there is less
8 information on where transcription-related processes take place *in vivo*, and how the
9 different structures involved change their architecture in response to cell requirements
10 during different developmental programs.

12 The nuclear space separating chromosome territories is the interchromatin region
13 (IR). At the boundaries of the IR with the condensed chromatin, decondensed chromatin
14 fibers are being transcribed to RNA in the form of perichromatin fibrils (PFs). PFs are short
15 fibers of 3-5 nm in diameter, present in a dispersed pattern through the perichromatin
16 region. They are thought to be the visible evidence of nascent pre-mRNA coupled to the co-
17 transcriptional splicing machinery (Monneron and Bernhard, 1969; Testillano et al., 1993;
18 Cmarko et al., 1999; Fakan, 2004). In addition, the IR houses the different structures
19 involved on post-translational regulatory steps such as RNA processing and nuclear protein
20 modification (Cremer and Cremer, 2001).

22 Once the pre-mRNA (hnRNA) sequence is generated in the form of a PF, three
23 subdomains are proposed as directly or indirectly involved in pre-mRNA splicing,
24 processing and transport: interchromatin granules, Cajal bodies and perichromatin

1
2
3
4
5
6
7
8
9
10
11
12
13
14
15
16
17
18
19
20
21
22
23
24
25
26
27
28
29
30
31
32
33
34
35
36
37
38
39
40
41
42
43
44
45
46
47
48
49
50
51
52
53
54
55
56
57
58
59
60
61
62
63
64
65

1 granules (Spector, 1993a; Raska, 1995; Lamond and Spector, 2003; Fakan, 2004).
2 Interchromatin granule clusters (IGCs) were found in mammalian (Puvion *et al.*, 1984) and
3 plant nuclei (Testillano *et al.*, 1993), and they are seen as ‘speckles’ under the fluorescence
4 microscope. They are interchromatin structures composed of 20-25 nm particles embedded
5 in a thin fibrillar matrix. Although different pre-mRNA splicing factors, including snRNPs
6 and SR proteins are present in IGCs, no DNA or transcriptional activity has consistently
7 been detected in these structures (Thiry, 1995; Cmarko *et al.*, 1999). Thus, IGCs are
8 currently considered as storage, assembly and modification compartments for the delivery
9 of transcription factors to active transcription sites (Lamond and Spector, 2003). Cajal
10 bodies (CBs) are universal, multifunctional, nearly round, convoluted and highly dynamic
11 structures frequently found associated to the nucleolus. snRNPs, the p80 coilin protein, the
12 U2AF splicing factor and diverse snRNAs have been detected in CBs, along with several
13 nucleolar proteins such as fibrillarin (reviewed in (Gall, 2000; Lafarga *et al.*, 2009).
14 However, poly-A RNA, rRNA, nascent mRNA transcripts, the SC-35 protein, DNA or
15 RNA polymerase II are not found in CBs, indicating that they are not directly involved in
16 transcription. Instead, it is believed that CBs are involved in the assembly and modification
17 of the machinery for processing of pre-mRNA, pre-rRNA and histone pre-mRNA (Gall,
18 2000; Matera, 2003; Shaw and Brown, 2004). Different studies have related the abundance
19 of CBs to cell activity (Andrade *et al.*, 1993), type (Raska *et al.*, 1991) and developmental
20 stage (Boudonck *et al.*, 1998). Although smaller and less conspicuous, the perichromatin
21 granules (PGs) are also integral components of the eukaryotic nucleus. RNA processing,
22 altered transport, storage and/or degradation of specific RNAs is thought to be mediated by
23 PGs (Puvion and Lange, 1980; Vazquez-Nin *et al.*, 1997).

1
2
3
4 1 As evidenced in most of the literature above cited, the knowledge on *in vivo*
5
6 2 functional organization of the different subnuclear structures involved in transcriptional
7
8 3 regulation has traditionally been derived, to a great extent, from studies on animal nuclei.
9
10 4 Comparatively, the plant nucleus has been less studied. In order to contribute to the
11
12 5 knowledge on the relationship between plant nuclear remodeling and expression patterns, in
13
14 6 this work we analyzed the changes in nuclear architecture during two different
15
16 7 developmental programs, involving proliferation and differentiation. We studied *Brassica*
17
18 8 *napus* embryogenesis-induced microspores and maturing pollen grains. In microspores, we
19
20 9 induced an embryogenic developmental program defined by a initial, proliferative phase
21
22 10 with increased transcriptional activity (reviewed in (Seguí-Simarro and Nuez, 2008). In
23
24 11 parallel, we studied pollen differentiation, characterized by the formation of a moderately
25
26 12 active vegetative cell, and a generative cell transcriptionally silent (Bednarska, 1984).
27
28
29
30
31
32
33
34
35

36 14 The comparative study of microspores and pollen grains committed to proliferative
37
38 15 and differentiation events constitutes a good model to study cellular changes related to a
39
40 16 developmental reprogramming (Seguí-Simarro et al., 2003, 2005; Barany et al., 2010). In
41
42 17 this study, we focused on the changes pertaining to the nuclear structures of the
43
44 18 interchromatin domain (perichromatin fibrils, interchromatin granules, Cajal bodies and
45
46 19 perichromatin granules). Our results indicated that a remodeling of the interchromatin
47
48 20 structures accompanied the change of developmental program of the microspores, being
49
50 21 those changes related to proliferation and differentiation events. The results also reveal two
51
52 22 novel structural domains, not previously described in plants, and point to the notion that the
53
54 23 different availability and abundance of these structures may serve as a regulatory
55
56 24 mechanism operating at a post-transcriptional level.
57
58
59
60
61
62
63
64
65

1
2
3
4 1 **Material and methods**
5
6
7 2

8
9 3 *Plant material*
10

11 4 *Brassica napus* L. cv Topas donor plants were grown as previously described
12
13
14 5 (Seguí-Simarro et al., 2003). Microspore cultures, embryogenesis induction, and sampling
15
16 6 at specific culture stages for light and electron microscopy, immunofluorescence, and
17
18 7 immuno-gold labelling were performed essentially according to (Seguí-Simarro et al.,
19
20
21 8 2003), with some modifications to promote the suspensor-bearing embryogenic route as
22
23 9 described (Supena et al., 2008). For the study of pollen development, anthers at different
24
25
26 10 developmental stages were selected and excised from plants.
27
28
29 11

30
31 12 *Electron microscopy and ultrastructural cytochemistry*
32

33 13 Samples to be observed for electron microscopy were fixed in Karnovsky fixative
34
35
36 14 (4% formaldehyde + 5% glutaraldehyde in 0.025M cacodilate buffer, pH 6.7), post-fixed in
37
38 15 2% OsO₄, dehydrated in a methanol series for 3 days and slowly embedded in Epon resin
39
40
41 16 for 2 days. Epon blocks were polymerized at 60°C for 2 days. ~80 nm-thick sections were
42
43 17 collected on 75-mesh copper grids, counterstained with uranyl acetate and lead citrate and
44
45 18 observed in a JEOL 1010 TEM operating at 80 kV. For the study of the different structures
46
47
48 19 present in the interchromatin region, the methylation-acetylation (MA) and the EDTA
49
50
51 20 cytochemical methods were used, either separately or combined. For the preferential
52
53 21 staining of DNA, the NAMA-Ur (Testillano *et al.* 1991) ultrastructural cytochemistry was
54
55 22 used. The MA method is a preembedding technique that highlights nucleic acid-containing
56
57
58 23 structures (fibrillar and granular) by a selective blockage of the protein ability to react with
59
60 24 uranyl acetate (Testillano *et al.*, 1995). For this method, fixed samples were dehydrated in a
61
62
63
64
65

1
2
3
4
5
6
7
8
9
10
11
12
13
14
15
16
17
18
19
20
21
22
23
24
25
26
27
28
29
30
31
32
33
34
35
36
37
38
39
40
41
42
43
44
45
46
47
48
49
50
51
52
53
54
55
56
57
58
59
60
61
62
63
64
65

1 methanol series and incubated in a freshly made methanol:acetic anhydride mixture (5:1
2 v:v) overnight at room temperature, prior to embedding. After three washings with
3 methanol, samples were embedded in Epon as described. For NAMA-Ur cytochemical
4 method, fixed samples were subjected to a mild alkaline hydrolysis with NaOH to eliminate
5 RNA, followed by MA treatment and Epon embedding; subsequent uranyl staining of the
6 sections result in a preferential staining of DNA containing structures (Testillano *et al.*
7 1991). The EDTA regressive staining (Bernhard, 1969) is used over EM sections to provide
8 RNP-containing structures a preferential staining over the bleached masses of condensed
9 chromatin. Samples fixed in 4% formaldehyde, dehydrated by the PLT (Progressive
10 Lowering of Temperature) method in a Leica AFS automatic system, and embedded in
11 Lowicryl K4M, resin were used for this cytochemical method.

12
13 *Cryoprocessing of samples for cryomicrotomy and immunofluorescence*

14 Microspore and microspore-derived embryo cultures were cryoprocessed for
15 cryomicrotomy and cryosectioned as previously described (Seguí-Simarro *et al.*, 2003).
16 Microspore cultures were slightly prefixed in 4% formaldehyde at 4°C and embedded in
17 gelatin. Small (1 mm³) pieces of gelatin were cryoprotected with increasing concentrations
18 of sucrose: 0.1M (1 h), 1M (3 h), and 2.3M (overnight), placed on an aluminum pin and
19 cryofixed in liquid propane using a KF80 unit (Reichert, Vienna) at -170°C. Thin (1 µm
20 thick) cryosections were obtained using an Ultracut E (Reichert) ultramicrotome coupled
21 with a FC4 unit stabilized at -75°C. Cryosections were collected and placed on multiwell
22 glass slides for immunofluorescence. Immunofluorescence was also performed essentially
23 as described (Seguí-Simarro *et al.*, 2003), with the primary mouse monoclonal antibody
24 anti-2,2,7-tri-methyl-guanosine, TMG (Calbiochem, clone K121) diluted 1/100 and

1 incubated for 1 h at room temperature, and the secondary antibody (anti-mouse IgG-Cy3)
2 diluted 1:25 in 1% BSA in PBS, and incubated for 45 min. Sections were additionally
3 stained with DAPI prior to observation. Controls were performed excluding the primary
4 antibody.

6 *Immunoelectron microscopy*

7 Microspores and haploid embryos at different stages were prefixed in
8 formaldehyde, cryoprotected in 2.3M sucrose, cryofixed in liquid nitrogen, and
9 cryoprocessed as described (Seguí-Simarro et al., 2003). Samples were freeze-substituted in
10 methanol + 0.5% uranyl acetate at -80°C for 3 days, infiltrated in Lowicryl K4M, and
11 polymerized at -30°C under UV light in a Leica AFS system. Ultrathin (80 nm) sections
12 were placed on nickel grids, blocked with 5% BSA in PBS, and incubated with anti 2,2,7-
13 TMG diluted 1/100 for 1h at room temperature. Then, the grids were incubated with a
14 secondary antibody (anti-mouse IgG -gold, 10 nm; Biocell) diluted 1:25 in 1% BSA, for 45
15 min at room temperature, washed, air dried, counterstained, and observed in a JEOL 1010
16 EM at 80 kV. Controls were performed excluding the primary antibody.

18 *Morphometric and quantitative analysis*

19 Sampling was carried out over selected samples on each grid. The number of
20 micrographs to be taken was determined by the progressive mean test (Williams, 1977),
21 with a maximum confidence limit of $\alpha=0.05$. Digital images of cells showing one or more
22 CBs were processed with the ImageJ software (<http://rsbweb.nih.gov/ij/>) for the
23 morphometric analysis of numbers, areas, and distances. Data were exported to a
24 spreadsheet where the final calculations and chart displays were performed.

Results

The first step of the study was the selection of the most representative stages of microspore embryogenesis and pollen development to be processed and analyzed. For microspore-derived embryogenesis, we chose the earliest stages, immediately before and after embryogenesis induction, where the most dramatic rearrangements at the structural, ultrastructural and molecular levels have been described (Maraschin et al., 2005; Seguí-Simarro and Nuez, 2008). These stages comprise: (1) vacuolate microspores and young bicellular pollen just extracted from the anther but prior to exposure to the inductive heat shock (Figure 1A, 2A) and (2) just after induction (Figure 1B), where the first sporophytic divisions are seen still within the exine coat (inset in Figure 1B); (3) induced, early microspore-derived embryos (MDEs; Figure 1C), once released from the exine coat and with two clearly differentiated suspensor and embryo proper domains; (4) globular MDEs (Figure 1D), where the first signs of tissue differentiation are visible in the embryo proper domain (inset in Figure 1D); and (5) heart-shaped MDEs (Figure 1E, 2B), where the embryo pattern of symmetry changes from radial to bilateral, hypocotyl and cotyledon begin to elongate and differentiation of internal tissues takes place (Tykarska, 1980). For pollen development, we selected (1) the vacuolate microspore, before the first pollen mitosis, (2) the young pollen grain (Figure 3A) immediately after the first pollen mitosis, (3) the mid pollen grain (Figure 3B), when the generative cell displaces towards the center of the vegetative cell, and (4) the late, mature pollen grain (Figure 3C), when sperm cells are formed after the second pollen mitosis, still within the anther locule.

Nuclear size, chromatin condensation pattern and nucleolar architecture

The nucleus of vacuolate microspores was typically round or slightly oval, large and off-centered (Figures 1A inset, 2A) due to the presence of a large central vacuole. Chromatin displayed the decondensed pattern typical of this species, with only few, large masses of condensed chromatin often associated to the inner side of the nuclear envelope (Figure 2A), allowing for an abundant interchromatin region. In induced microspores, the first embryogenic division was symmetric and gave rise to two similar nuclei, equivalent in size (Figure 6C), rounded and centrally positioned. Subsequent divisions of the embryo proper cells produced progressively smaller nuclei (Figure 4A). This nuclear morphology was observed, with slight differences, in interphasic nuclei of microspores and MDEs through the early stages of embryogenesis. The chromatin pattern in these cells could be defined as dark, electron dense masses in electron microscopy sections of samples treated with the nucleic acid-contrasting MA cytochemistry (Figures 2A, 2B), as clear, bleached masses (Figure 5A) in sections treated with the EDTA regressive cytochemical staining, or as intense, peripheral bright spots in nuclei stained with the fluorescent, DNA-specific DAPI staining (Figures 6A-D).

This pattern strikingly contrasted with that observed in developing pollen under non-inductive conditions (Figure 3). Immediately after the first pollen mitosis (Figure 3A), a large, vegetative (VN) and a smaller, generative nucleus (GN) appeared within the vegetative and generative cells. As pollen maturation proceeded, the VN retained an architecture comparable to that described for vacuolate microspore nuclei (compare Figures 3B-B', 2A). However, as the generative cell moved from the periphery to the center of the

1
2
3
4
5
6
7
8
9
10
11
12
13
14
15
16
17
18
19
20
21
22
23
24
25
26
27
28
29
30
31
32
33
34
35
36
37
38
39
40
41
42
43
44
45
46
47
48
49
50
51
52
53
54
55
56
57
58
59
60
61
62
63
64
65

1 vegetative cell, the size of the GN dramatically decreased (Figure 3B; 4B) and chromatin
2 adopted a highly condensed status, appearing as large bleached masses after EDTA staining
3 (Figure 3B’). In the mature pollen grain, the VN showed signs of increased chromatin
4 condensation (Figure 3C’), while the nuclear envelope adopted irregular, lobed
5 morphologies (Figure 3C). After the second pollen mitosis, the two newly formed sperm
6 nuclei occupied nearly all of the volume of the sperm cells (Figure 3C). Chromatin
7 condensation reached the highest levels, appearing in MA-treated samples as large, densely
8 stained masses (Figure 3C) and as bleached areas in EDTA samples (Figure 3C’’).

9
10 It is well established that changes in the transcriptional status of the cell are
11 accompanied by significant extensive changes in nucleolar volume and morphology.
12 (Raska et al., 1983; Goessens, 1984). Thus, in this work we used the nucleolar organization
13 as a reliable marker to identify cells at different transcriptional status. At the vacuolate
14 microspore stage, the nucleolus was round, centered, large with respect to the total nuclear
15 volume (Figure 2A), and displaying a torus-shaped profile typical of highly active cells: a
16 large central vacuole with ribonucleoprotein particles (RNPs), and abundant granular
17 component (GC) intermingled with dense fibrillar component (DFC). In the DCF, many
18 small and homogeneous fibrillar centers (FCs) were observed (Figure 2A). In MDEs, the
19 nucleolar architecture appeared more variable. Indeed, besides the torus-shaped profiles
20 indicative of highly active nucleoli, profiles indicative of moderate and low activity were
21 also observed in other cells. Profiles of moderate activity were defined by the presence of
22 many small, homogeneous FCs within a DFC with abundant GC (data not shown). Low
23 activity profiles included few, large and heterogeneous FCs, and scarce GC, usually located
24 at the periphery of the DFC (Figure 2B). During pollen development, the nucleolus of the

1 generative cell frequently showed low activity profiles just after the first pollen mitosis
2 (Figure 3A), whereas profiles of moderate activity were evident in the vegetative nucleus
3 up to the mid pollen stage (Figure 3B). In mature pollen grains, the nucleolus was reduced
4 to a compact, dense and inactive structure in the generative nucleus and in sperm cells
5 (Figure 3C). In the vegetative nucleus, nucleoli were visible up to the mid pollen stage.

6 7 **Cytochemical analysis of the interchromatin region**

8
9 In MA-treated samples, condensed chromatin masses showed higher contrast than
10 the nucleolus and interchromatin RNP structures (Figure 5A), being the chromatin patches
11 clearly defined. EDTA nuclear staining revealed some interesting and novel features of the
12 plant IR. At a first visual inspection, the areas of EDTA-bleached, condensed chromatin
13 masses (Figure 5B) were found apparently larger than their equivalents in MA (non-EDTA)
14 treated samples (Figure 5A). To verify this observation, we quantitatively evaluated the
15 areas of large chromatin masses in 100 randomly chosen MDE cells from EDTA and MA
16 treated sections. We found that the average area of a bleached chromatin region in EDTA-
17 stained samples was $0.47 \pm 0.29 \mu\text{m}^2$, whereas in MA stained samples it was 0.37 ± 0.23
18 μm^2 . This difference (~21%) indicated that EDTA bleaches not only chromatin masses, but
19 also the adjacent, perichromatin region where probably abundant chromatin fibres of
20 different thickness are preferentially located. The use of the NAMA-Ur cytochemical
21 method, preferential for DNA (Testillano et al. 1991), clearly revealed stained numerous
22 chromatin fibres of different thicknesses at the periphery of the chromatin masses (Figure
23 5C, arrows). The comparison of these cytochemical techniques suggested the existence of a
24 perichromatin region, rich in decondensed chromatin.

1 EDTA also revealed the presence of a dense fibrillo-granular RNP network filling
2 the nucleoplasmic space between chromatin masses. In all of the embryogenic and
3 gametophytic stages studied, we observed the presence of perichromatin fibrils (9.9 ± 1.24
4 nm wide), either emerging from the mass borders or as isolated threads embedded in the IR
5 (Figure 6B). Isolated granules, 37.8 ± 5.96 nm in diameter, were observed dispersed through
6 the IR, mostly in induced microspores and MDEs. They were frequently seen at the nuclear
7 periphery, close to the nuclear envelope (Figures 6D, E). Their size, spherical shape,
8 staining properties and principally the presence of a defined halo around them, allowed us
9 to identify them as perichromatin granules according to (Monneron and Bernhard, 1969).

11 Smaller (22.3 ± 5.53 nm in diameter) spherical granules were also found in the IR
12 (Figures 6A, C), both isolated and grouped into clusters over a fibrillar matrix (Figure 5C).
13 According to their distribution, these granules were likely interchromatin granules (IG).
14 Correspondingly, clustered IGs would be interchromatin granule clusters (IGCs), the
15 electron microscopy equivalents of the nuclear speckles observed by fluorescence
16 microscopy (Lamond and Spector, 2003). In some sections we were able to identify a
17 clearer, mostly fibrillar region devoid of IGs but always adjacent to IG clusters (Figure 6C,
18 dotted lines). The structure of these regions highly resembled the “interchromatin granule-
19 associated zone” previously described in mammalian cells (Visa et al., 1993).

21 IGCs were evident throughout microspore embryogenesis. First in dividing
22 microspores, and to a lower extent in MDEs. During pollen development, IGCs were
23 observed soon after the first pollen mitosis (Figures 3A-A’). However, their presence was
24 progressively reduced during pollen maturation. Isolated IGs were observed as dark, well

1 defined, isolated particles through the progressively reduced IR of the early (Figures 3A-
2 A''), mid (Figures 3B-B'') and finally mature pollen grain (Figures 3C-C''). This was
3 paralleled by a progressive decrease in nuclear size and a remarkable increase in the
4 condensation status of chromatin. The intensity of the transformations was higher in the
5 generative nuclei, GNs (compare Figures 3B-B''), and in sperm cells (Figure 3C''), and
6 with less intensity in the vegetative nuclei, VNs. In summary, these results indicated a
7 relationship between the increase in chromatin condensation, the IR reduction and a change
8 in the distribution pattern of IGs from clustered to isolated, during pollen maturation.

9 10 **Nuclear immunolabeling with anti 2,2,7 – trimethylguanosine**

11
12 Further characterization of the IR substructures involved immunolabeling with
13 antibodies against 2,2,7-trimethylguanosine (TMG), the specific cap present in the RNA of
14 the small nuclear RNPs (snRNPs). SnRNPs are major components of the splicing
15 machinery (Lührmann, 1988). Anti-TMG signal was observed in all of the embryogenic
16 stages studied during MDE development. Immunofluorescence signal (Figure 7) was
17 located at the nucleus in the form of a faint signal and some discrete, round and intensely
18 bright foci. These foci never colocalized with those observed for DAPI staining (compare
19 Figures 7A-E and 7A'-E'), indicating that chromatin is excluded from them. The nucleolus
20 always appeared devoid of fluorescence as well, indicating that these structures were
21 confined to the IR and most probably corresponded to nuclear bodies. During pollen
22 maturation, the faint fluorescence was negligible, and very few foci could be observed after
23 the first pollen mitosis, mainly in the VN (Figure 7B'). As the chromatin of the pollen
24 nuclei condensed, the TMG-labeled structures were less evident, becoming no longer

1 detectable in mature pollen (Figure 3C). Therefore, we focused on the study of these
2 structures during MDE development, where intense foci were present (Figure 7C-E').

3
4 Anti-TMG immunogold labeling confirmed a faint labeling throughout different
5 regions of the IR. At the boundaries between the chromatin masses and the IR, significant
6 labeling was found (Figure 8C, arrowheads), possibly detecting snRNPs associated to
7 nascent transcripts. The nucleolus was nearly devoid of labeling. Labeling of the IR
8 appeared either as isolated particles or as clusters of few (2-6) particles (Figures 8A-C). By
9 combining immunogold labeling with EDTA staining it was shown that particle clusters
10 decorated EDTA-positive, RNP-containing IR regions (Figure 8D, arrows), in a pattern
11 similar to that described for IGCs. Thus, the clusters of gold particles of the IR would
12 actually correspond to the granular IGC regions observed in Epon-embedded samples,
13 although with a different appearance, due to the different processing, as described
14 previously in other studies of the IR (Testillano et al., 1993).

15
16 In addition to small clusters, immunogold particles concentrated massively over
17 dense, coiled-looking bodies (Figures 8A-E) that according to their size and position
18 corresponded to the bright foci observed with immunofluorescence. These bodies
19 frequently exhibited a nearly circular section, variable in size, and a thick fibrillar texture
20 embedded into a light matrix continuous with the IR. Immunogold labeling decorated RNP-
21 positive, particle-like structures contained within the matrix of the body (Figure 8D). The
22 structure, size, nature and position of these bodies, together with the labeling with anti
23 TMG, indicative of presence of RNPs, are characteristics of Cajal Bodies (CBs; (Fakan et
24 al., 1984; Spector et al., 1991; Spector, 1993a; Seguí-Simarro et al., 2006). In addition,

1 where the sectional plane was appropriate, we could also observe a clearer, homogeneous
2 and scarcely labeled region associated to the CB (cb-az in Figure 8E), and structurally
3 different from other subnuclear structures. The structural characteristics of these novel
4 regions, not described to date in plants, resembled the *cleavage bodies* described as
5 associated to CBs in animal cells (Schul et al., 1996; Gall, 2000).

6 7 **Qualitative and quantitative analysis of Cajal bodies**

8
9 According to the criteria exposed above, we identified CBs in all of the
10 embryogenic stages studied. Interestingly, in freshly isolated microspores we noticed a
11 relatively lower electron density of CBs compared to CBs of other stages (compare Figures
12 8A and 8B). Most of the CBs in just induced microspores (not shown) and early globular
13 MDEs (Figure 8B) presented in general a similar appearance in terms of electron density
14 (high) and circularity (reduced). In late globular and heart-shaped MDEs, circular, electron
15 light CBs were more abundant.

16
17 For the quantitative analysis of CBs, we first estimated the number (Figure 9A) and
18 area (Figure 9B) of CBs at each stage in order to have a clear view of their abundance
19 during MDE development. Given the differences in nuclear size at different stages (Figure
20 2C), we normalized the nuclear density and size of CBs expressing them as number or area
21 of CBs per nuclear μm^2 . Figure 9A shows that microspores prior to induction presented
22 comparatively less CBs than any other stage. Commitment of microspores to
23 embryogenesis was paralleled by an increase in the number of CBs, peaking in early
24 globular MDEs. In late globular and heart-shaped MDEs, when tissue differentiation starts,

1
2
3
4
5
6
7
8
9
10
11
12
13
14
15
16
17
18
19
20
21
22
23
24
25
26
27
28
29
30
31
32
33
34
35
36
37
38
39
40
41
42
43
44
45
46
47
48
49
50
51
52
53
54
55
56
57
58
59
60
61
62
63
64
65

1 the number of CBs showed a similar, reduced value, slightly higher than in microspores. A
2 completely opposite trend was reflected in mean CB area calculations (Figure 9B). After
3 induction, the size of CBs was drastically reduced, increasing progressively through the
4 following stages of embryogenesis. Thus, an inverse relationship between CB size and
5 number follow was evident (compare the trend lines of Figures 9A and 9B). After
6 measuring the total area occupied by CBs at each stage (Figure 9C), we could confirm this
7 relationship by observing that the total area was nearly constant except for one stage. In
8 induced microspores, the total CB area was remarkably lower.

9
10 An additional unexpected finding arose when we compared the error bars of the
11 different stages. Since the measured area of a nearly spherical object like a CB depends on
12 the sectional plane, one would expect an error proportional to the measured area, and
13 similar for all of the stages. However, in freshly isolated microspores, the error was
14 comparatively smaller than in the other stages, suggesting that CBs in this stage are larger
15 and more uniform in size. To check this out, we analyzed the frequency distribution of the
16 areas of all of the CBs from the different stages considered altogether (Figure 9D). We
17 found that areas did not exhibited a gaussian distribution, as expected for a uniform size.
18 Instead, they showed a bimodal pattern, with measurements congregating around two peaks
19 at 0.15 and 0.35 μm^2 , which would correspond to estimated diameters of 0.44 and 0.67 μm ,
20 respectively. Thus, it appeared that CBs may have two different sizes, large and small,
21 which according to our micrograph analysis correspond to the electron light (Figure 9E)
22 and electron dense (Figure 9F) types above described, respectively. CBs of freshly isolated
23 microspores would belong almost exclusively to the large and electron light type, whereas
24 after induction both types may coexist, being the small more frequent in early post-

1
2
3
4
5
6
7
8
9
10
11
12
13
14
15
16
17
18
19
20
21
22
23
24
25
26
27
28
29
30
31
32
33
34
35
36
37
38
39
40
41
42
43
44
45
46
47
48
49
50
51
52
53
54
55
56
57
58
59
60
61
62
63
64
65

1 inductive stages and the large more frequent in later embryogenic stages. Once established
2 two different CB categories, we reexamined the presence of the CB-associated zones, and
3 interestingly, they were exclusively found associated with CBs of the small and dense type.
4 In summary, it appeared that CBs change their size, number, shape, and position in a
5 defined manner during early MDE development, whereas they disappear during pollen
6 maturation. These data would be indicating that the described changes are a reflection of
7 the change in developmental program.

8
9

1
2
3
4 **1 Discussion**
5
6
7
8
9
10
11
12
13
14
15
16
17
18
19
20
21
22
23
24
25
26
27
28
29
30
31
32
33
34
35
36
37
38
39
40
41
42
43
44
45
46
47
48
49
50
51
52
53
54
55
56
57
58
59
60
61
62
63
64
65

1
2
3
4 **1 Discussion**
5
6
7
8
9
10
11
12
13
14
15
16
17
18
19
20
21
22
23
24
25
26
27
28
29
30
31
32
33
34
35
36
37
38
39
40
41
42
43
44
45
46
47
48
49
50
51
52
53
54
55
56
57
58
59
60
61
62
63
64
65

4 The comparison between the gametophytic and sporophytic pathways followed by
5 the microspore permitted us to analyse the remodelling of the nuclear domains in plant
6 differentiating cells when switched to proliferation. The change of the developmental
7 program and the activation of the proliferative activity affected the functional organization
8 of the interchromatin domain, which accordingly changed their architecture and functional
9 state, and redistributed its components. A summary of the main nuclear changes observed
10 is shown in figure 10.

11
12
13
14
15
16
17
18
19
20
21
22
23
24
25
26
27
28
29
30
31
32
33
34
35
36
37
38
39
40
41
42
43
44
45
46
47
48
49
50
51
52
53
54
55
56
57
58
59
60
61
62
63
64
65

11
12 In this work, we present an ultrastructural, cytochemical and immunocytochemical
13 characterization of the changes in nuclear architecture, with special attention to the IR-
14 housed structures, during two different developmental processes with the same starting
15 point: differentiation of microspores into mature, gamete-harboring pollen grains,
16 transcriptionally inactive (Bednarska, 1984), and proliferation of embryogenesis-induced
17 microspores during the first embryogenic stages, highly engaged in transcription (Joosen et
18 al., 2007; Malik et al., 2008). The comparison of the changes undergone by the structures of
19 the IR during these two processes allowed us (1) to relate the remodeling of the
20 interchromatin domain to the change of developmental program and to variations in
21 transcriptional activities, and (2) to reveal novel features of the plant nucleus, not yet
22 described.

1
2
3
4 1 **Changes in chromatin pattern parallel the change of developmental program**
5
6
7 2
8
9 3

10 Numerous studies have shown a direct relationship between nuclear architecture and
11 the level of cellular activity (Risueño and Testillano, 1994; González-Melendi et al., 1998;
12 Testillano et al., 2000, 2005; Raska et al., 2004). In this work, we showed that the
13 chromatin pattern is also affected by the induction of microspore embryogenesis in *B.*
14 *napus*, constituting a good marker of developmental fate. In *B. napus* microspores
15 committed to embryogenesis, all nuclei show a similar decondensed chromatin pattern,
16 allowing for an abundant IR. The scarce chromatin masses are present mostly associated to
17 the nuclear envelope. This pattern, similar to that of somatic cells, could be considered as a
18 variation of the chromomeric condensation pattern (Jordan et al. 1980). This pattern
19 changes in pollen cells, where a strikingly different, highly condensed chromatin pattern is
20 observed. The embryogenic switch originates in the microspore and MDEs a characteristic
21 organization with less condensed chromatin pattern the chromatin, typical of proliferating
22 cells, and markedly different from developing microspores not committed to
23 embryogenesis.
24
25
26
27
28
29
30
31
32
33
34
35
36
37
38
39
40
41
42
43
44
45
46
47 18 **Changes in IR structures associated to induction of embryogenesis**
48
49
50
51
52 19
53
54 20
55
56
57 21
58
59 22
60
61
62
63
64
65

66 In this work, we have shown evidences of a remodeling of the IR-housed structures
67 as a consequence of the developmental switch of the induced microspore. IGs change from
68 grouped as IGCs mostly in dividing microspores (transcriptionally active), to isolated in
69 maturing pollen and gametes (transcriptionally inactive). In mammalian cells, various

1
2
3
4
5
6
7
8
9
10
11
12
13
14
15
16
17
18
19
20
21
22
23
24
25
26
27
28
29
30
31
32
33
34
35
36
37
38
39
40
41
42
43
44
45
46
47
48
49
50
51
52
53
54
55
56
57
58
59
60
61
62
63
64
65

1 reports showed that a transcription blockage resulted in the accumulation of splicing factors
2 in larger speckles/IGCs (Spector et al., 1983, 1991; Melcak et al., 2000; Docquier et al.,
3 2004). Nevertheless, in plant cells the organization of the IGs slightly differs. IGs have
4 been observed as isolated granules in many plant cell systems (Testillano et al. 1993), being
5 the splicing factors distribution more spread throughout the IR, as revealed by
6 immunofluorescence assays. In the generative and sperm cells, the nuclear size
7 progressively decreases as the chromatin adopts an extremely condensed pattern, which
8 dramatically reduces the space available for the IR to a minimal amount (Figures 3B'',
9 C''). This lack of space may likely be affecting IGC nucleation. In Arabidopsis trichome
10 cells, with extremely high endoreduplication levels, a transcription blockage causes the
11 appearance of thousands of microspeckles, instead of the expected larger speckles (Fang et
12 al., 2004). In parallel, the inconspicuous presence of IGCs in dividing microspores could
13 likely be related to the application of a heat shock treatment to induce the developmental
14 switch. Indeed, heat shock has been shown to promote the accumulation of plant splicing
15 factors in larger speckles/IGCs (Docquier *et al.*, 2004).

16
17 Other features of the IR, which were associated with the change of developmental
18 program, affected PGs and PFs. The increased number of PGs observed after the
19 embryogenesis-inductive heat-shock would support a similar role for plant PGs on the
20 accumulation of heat shock-damaged pre-mRNA molecules than in mammalian cells
21 (Puvion and Lange 1980). In HeLa cells (Chiodi et al., 2000) showed the formation of PG
22 clusters upon heat shock exposure. However, we could not identify such a clustered pattern
23 in any of our plant samples. EDTA staining revealed a perichromatin region of
24 decondensed chromatin, rich in decondensed chromatin which would correspond to active

1 genes ready for transcription and/or replication. The RNP fibrils (PFs) were observed
2 further away from the chromatin masses, and would correspond to the different stages of
3 hnRNA transcription and processing. Moreover, we identified a distinct region of
4 ribonucleoproteic nature, structurally similar to the IG-associated zone (IG-AZ) of HeLa
5 cells (Visa et al., 1993). The IG-AZ is considered as a part of the nuclear matrix that
6 contains p80-coilin and U1 snRNA (but not U2), and is thus thought to be a reservoir of
7 spliceosome components (Puvion-Dutilleul et al., 1995). These zones have never been
8 described in plants before, and their presence in certain cells could be indicating a higher
9 transcriptional activity. Nevertheless, further structural and immunochemical studies would
10 be necessary to characterize the functional role of this nuclear region in plants.

11

12 **Novel features of plant Cajal Bodies**

13

14 The combination of anti-TMG immunolabeling with ultrastructural cytochemistry
15 allowed us to identify several novel features of the plant CB. One of them is the
16 identification of two ultrastructurally different types of CBs in *B. napus*. Despite of their
17 differences, our structural and quantitative data reveal a number of similarities between
18 them highly suggestive of a similar nature for both. Indeed, they may actually be the
19 divided and fused forms of a same subnuclear structure, since it is known that CBs are
20 highly dynamic structures, undergoing frequent movements from/to the nucleolus, and also
21 fission and fusion between them (Lafarga et al., 1998; Boudonck et al., 1999; Platani et al.,
22 2000; Navascués et al., 2004). This plasticity may be the origin of the heterogeneity in CB
23 structure found in the *B. napus* nucleus, as well as in other plant cell types such as maize

1 root cells (Docquier et al., 2004), heterogeneity also observed in some animal cells (Liu et
al. 2006).

We have identified a clearer, large CB-associated zone (Figure 7E) always contacting CBs of the small, dense type. These regions are structurally similar to those described in animal cells as CB-associated cleavage bodies. due to the presence of, among others, factors for the cleavage of the 3'-end of polyadenilated mRNAs (Schul et al., 1996; Gall, 2000). A role for cleavage bodies was proposed related to the processing of specific pre-mRNA subsets not found in their associated CBs (Schul et al., 1996). Since the functional role of CBs is similar in plant and animal cells, it is likely that these plant CB-associated zones could have a similar role as well, even though more studies, combining structural characterization with *in situ* molecular localization, are needed to further characterize this novel compartment. Ultrastructural studies have found CBs and IGs associated in proliferating plant cells (Moreno-Díaa de la Espina et al. 1982); since CBs are mobile bodies and we have found similar AZs associated to IGs, the possibility that the three structures, CBs, IGs and AZ were associated cannot be excluded, even though it is very difficult to find the three in the same section.

It is known that the number of CBs in a cell is developmentally and cell cycle-regulated (reviewed in (Shaw and Brown, 2004), cell type-specific (Raska et al., 1991) and tightly related to the changes in transcriptional and metabolic activity (Carmo-Fonseca et al., 1992; Spector, 1993b). Our results showed that the number and size of CBs are tightly related to proliferation, in a direct manner for number, and inversely for size. The opposite scenario would apply for the relationship between CB size and number during

1
2
3
4
5
6
7
8
9
10
11
12
13
14
15
16
17
18
19
20
21
22
23
24
25
26
27
28
29
30
31
32
33
34
35
36
37
38
39
40
41
42
43
44
45
46
47
48
49
50
51
52
53
54
55
56
57
58
59
60
61
62
63
64
65

1 differentiation events. The only exception to this trend was observed in induced
2 microspores exiting from a recently applied heat shock, where clear deviations were
3 observed in individual and total CB size (Figs. 9B, C). Indeed, exposure to a heat shock
4 induces the formation of smaller CBs in different animal cells (Handwerger *et al.*, 2002;
5 Carmo-Fonseca *et al.*, 1992; 1993). Similar evidences have also been observed in HeLa
6 cells, where exposure to high temperatures produced smaller CBs, even losing their
7 contents in snRNPs

9 It has been proposed in sugarcane root primordial cells a model where the number
10 of CBs per nucleus would be fixed for a given species and cell type, independent of its
11 activity (Acevedo *et al.*, 2002). Our results would be in agreement with this notion,
12 provided that what remains constant is the total “mass” of CBs, not only their number, and
13 under non-stressing conditions. Taken together, these results would be indicating that the
14 total CB “mass” within a nucleoplasm remains nearly constant during MDE development in
15 the absence of stress. Upon stressing the cell, CBs would fragment into mini-CBs and
16 dismantle, but in a reversible manner, recovering the total CB “mass” the normal levels
17 after stress..

18
19 **Concluding remarks**

20
21 In this work we have shown that the different structures involved in RNA
22 processing change their shape and distribution in a characteristic manner as a consequence
23 of the reprogramming of the microspore from the natural, gamete-producing route to the in
24 vitro, embryo-producing route. Some features of the IR were heat shock-derived

1 consequences. After heat shock CBs reduce considerably their individual size and their
2 total volume, although in a reversible manner. The increased occurrence of IGCs in induced
3 microspores could also be a heat shock effect.

4
5 Other IR changes were associated with the commitment to proliferation (in MDEs)
6 or to differentiation (in maturing pollen). The change of IR volume, the distribution pattern
7 of IGs, and the number and size of CBs were related to a change in the transcriptional status
8 of the cell. Moreover, novel features of plant IR-housed structures have been found, such as
9 the presence of two IR zones specifically associated to IGCs and CBs, the existence of
10 heterogeneity in the structure of the plant CB, with a smaller and denser type, and a larger
11 and lighter type. A significant remodelling of the microspore transcriptome has been
12 recently described as a essential part of the microspore switch to embryogenesis (Hosp *et*
13 *al.*, 2007a, 2007b; Joosen *et al.*, 2007; Malik *et al.*, 2007). While chromosome remodelling
14 during reprogramming (Hosp *et al.*, 2007a) would act as a pre-translational mechanism for
15 regulation of gene expression, the changes described in the present work of the structures
16 associated to RNA processing machinery would serve as a first post-translational regulatory
17 mechanism.

18 19 **Acknowledgements**

20 This work was supported by grants from the Spanish Ministry of Education and
21 Science AGL2006-06678 to JMSS, AGL2008-04255 to MCR BFU2008-00203 to PST and
22 Czech grants MSM0021620606, LC535 and AV0Z50110509 to IR.

References

- Acevedo, R., Samaniego, R., de la Espina, S.M.D. 2002.** Coiled bodies in nuclei from plant cells evolving from dormancy to proliferation. *Chromosoma* 110: 559-569.
- Andrade, L.E., Tan, E.M., Chan, E.K.L. 1993.** immunocytochemical analysis of the coiled body in the cell cycle and during proliferation. *P.Natl. Acad. Sci. USA* 90: 1951.
- Barany, I., Fadon, B., Risueno, M.C., Testillano, P.S. 2010.** Cell wall components and pectin esterification levels as markers of proliferation and differentiation events during pollen development and pollen embryogenesis in *Capsicum annuum* L. *J. Exp. Bot.* 61: 1159-1175.
- Bednarska, E. 1984.** Ultrastructural and metabolic transformations of differentiating *Hyacinthus orientalis* L. pollen grain cells. I. RNA and protein synthesis. *Acta Societatis Botanicorum Poloniae* 53: 145-158.
- Bernhard, W. 1969.** A new staining procedure for electron microscopical cytology. *J. Cell. Sci.* 27: 250-265.
- Boudonck, K., Dolan, L., Shaw, P.J. 1998.** Coiled body numbers in the Arabidopsis root epidermis are regulated by cell type, developmental stage and cell cycle parameters. *J. Cell. Sci.* 111: 3687-3694.
- Boudonck, K., Dolan, L., Shaw, P.J. 1999.** The movement of coiled bodies visualized in living plant cells by the green fluorescent protein. *Mol. Biol. Cell* 10: 2297-2307.
- Carmo-Fonseca, M., Ferreira, J., Lamond, A.I. 1993.** Assembly of snRNP-containing coiled bodies is regulated in interphase and mitosis - evidence that the coiled body is a kinetic nuclear structure. *J. Cell Biol.* 120: 841-852.
- Carmo-Fonseca, M., Pepperkok, R., Carvalho, M.T., Lamond, A.I. 1992.** Transcription-dependent colocalization of the U1, U2, U4/U6 and U5 snRNPs in coiled bodies. *J. Cell Biol.* 117: 14.
- Cmarko, D., Verschure, P.J., Martin, T.E., Dahmus, M.E., Krause, S., Fu, X.D., van Driel, R., Fakan, S. 1999.** Ultrastructural analysis of transcription and splicing in the cell nucleus after bromo-UTP microinjection. *Mol. Biol. Cell* 10: 211-223.
- Cremer, T., Cremer, C. 2001.** Chromosome territories, nuclear architecture and gene regulation in mammalian cells. *Nat. Rev. Genet.* 2: 292-301.
- Chiodi, I., Biggiogera, M., Denegri, M., Corioni, M., Weighardt, F., Cobianchi, F., Riva, S., Biamonti, G. 2000.** Structure and dynamics of hnRNP-labelled nuclear bodies induced by stress treatments. *J. Cell. Sci.* 113: 4043-4053.
- Docquier, S., Tillemans, V., Deltour, R., Motte, P. 2004.** Nuclear bodies and compartmentalization of pre-mRNA splicing factors in higher plants. *Chromosoma* 112: 255-266.
- Fakan, S. 2004.** Ultrastructural cytochemical analyses of nuclear functional architecture. *Eur. J. Histochem.* 48: 5-14.
- Fakan, S., Leser, G., Martin, T.E. 1984.** Ultrastructural distribution of nuclear ribonucleoproteins as visualized by immunocytochemistry of thin sections. *J. Cell Biol.* 98: 358-363.
- Fang, Y.D., Hearn, S., Spector, D.L. 2004.** Tissue-specific expression and dynamic organization of SR splicing factors in Arabidopsis. *Mol. Biol. Cell* 15: 2664-2673.
- Gall, J.G. 2000.** Cajal bodies: the first 100 years. *Annu.Rev.Cell Dev.Biol.* 16: 273-300.
- Goessens, G. 1984.** Nucleolar structure. *International Review of Cytology* 87: 107-158.

- 1 **González-Melendi, P., Testillano, P.S., Mena, C.G., Muller, S., Raska, I., Risueño,**
2 **M.C. 1998.** Histones and DNA ultrastructural distribution in plant cell nucleus: A
3 combination of immunogold and cytochemical methods. *Experimental Cell Research* 242:
4 45-59.
- 5 **Handwerger, K.E., Wu, Z.A., Murphy, C., Gall, J.G. 2002.** Heat shock induces mini-
6 Cajal bodies in the *Xenopus* germinal vesicle. *J. Cell. Sci.* 115: 2011-2020.
- 7 **Hosp, J., Maraschin, S.D.F., Touraev, A., Boutilier, K. 2007a.** Functional genomics of
8 microspore embryogenesis. *Euphytica* 158: 275-285.
- 9 **Hosp, J., Tashpulatov, A., Roessner, U., Barsova, E., Katholnigg, H., Steinborn, R.,**
10 **Melikant, B., Lukyanov, S., Heberle-Bors, E., Touraev, A. 2007b.** Transcriptional and
11 metabolic profiles of stress-induced, embryogenic tobacco microspores. *Plant Mol. Biol.*
12 63: 137-149.
- 13 **Jarillo, J.A., Piñeiro, M., Cubas, P., Martínez-Zapater, J.M. 2009.** Chromatin
14 remodeling in plant development *Int. J. Dev. Biol.* In press.
- 15 **Joosen, R., Cordewener, J., Supena, E.D.J., Vorst, O., Lammers, M., Maliepaard, C.,**
16 **Zeilmaker, T., Miki, B., America, T., Custers, J., Boutilier, K. 2007.** Combined
17 transcriptome and proteome analysis identifies pathways and markers associated with the
18 establishment of rapeseed microspore-derived embryo development. *Plant Physiol.* 144:
19 155-172.
- 20 **Jordan, E.G., Timmis, J.V., Trewaras, A.J. 1980.** The plant nucleus. In *The*
21 *Biochemistry of plants*. Vol1, ed. by N.E. Tolbert Academic Press. New York, London:
22 489-588.
- 23 **Lafarga, M., Casafont, I., Bengoechea, R., Tapia, O., Berciano, M.T. 2009.** Cajal's
24 contribution to the knowledge of the neuronal cell nucleus. *Chromosoma* 118: 437-443.
- 25 **Lamond, A.I., Spector, D.H. 2003.** Nuclear speckles: a model for nuclear organelles. *Nat.*
26 *Rev. Mol. Cell Biol.* 4: 605-612.
- 27 **Liu, J.-L., Murphy, C., Buszczak, M., Clatterbuck, S., Goodman, R., Gall, J.G. 2006.**
28 *The Drosophila melanogaster* Cajal body. *The Journal of Cell Biology* 172: 875-884.
- 29 **Lührmann, R. 1988.** snRNP proteins. In *Structure and function of major and minor*
30 *snRNPs*, ed. by M.L. Birnstiel Springer-Verlag. Berlin, Heidelberg: 71-99.
- 31 **Malik, M.R., Wang, F., Dirpaul, J.M., Zhou, N., Polowick, P.L., Ferrie, A.M.R.,**
32 **Krochko, J.E. 2007.** Transcript profiling and identification of molecular markers for early
33 microspore embryogenesis in *Brassica napus*. *Plant Physiol.* 144: 134-154.
- 34 **Malik, M.R., Wang, F., Dirpaul, J., Zhou, N., Hammerlindl, J., Keller, W., Abrams,**
35 **S.R., Ferrie, A.M.R., Krochko, J.E. 2008.** Isolation of an embryogenic line from non-
36 embryogenic *Brassica napus* cv. Westar through microspore embryogenesis. *J. Exp. Bot.*
37 59: 2857-2873.
- 38 **Maraschin, S.F., de Priester, W., Spaink, H.P., Wang, M. 2005.** Androgenic switch: an
39 example of plant embryogenesis from the male gametophyte perspective. *J. Exp. Bot.* 56:
40 1711-1726.
- 41 **Matera, A.G. 2003.** Cajal bodies. *Current Biology* 13: R503-R503.
- 42 **Melcak, I., Cermanova, S., Jirsova, K., Koberna, K., Malinsky, J., Raska, I. 2000.**
43 Nuclear pre-mRNA compartmentalization: Trafficking of released transcripts to splicing
44 factor reservoirs. *Mol. Biol. Cell* 11: 497-510.
- 45 **Monneron, A., Bernhard, W. 1969.** Fine structural organization of the interphase nucleus
46 in some mammalian cells. *Journal of Ultrastructural Research* 27: 288.

- 1
2
3
4 1 **Moreno Díaz de la Espina, S., Risueño, M.C., Medina, F.J. 1982.** Ultrastructural,
5 2 cytochemical and autoradiographic characterization of coiled bodies in the plant cell
6 3 nucleus. *Biol. Cell* 44: 229-238.
- 8 4 **Navascués, J., Berciano, M.T., Tucker, K.E., Lafarga, M., Matera, A.G. 2004.**
9 5 Targeting SMN to Cajal bodies and nuclear gems during neuritogenesis. *Chromosoma* 112:
10 6 398-409.
- 11 7 **Platani, M., Goldberg, I., Swedlow, J.R., Lamond, A.I. 2000.** In vivo analysis of Cajal
12 8 body movement, separation, and joining in live human cells. *J. Cell Biol.* 151: 1561-1574.
- 13 9 **Puvion-Dutilleul, F., Besse, S., Chan, E.K., Tan, E.M., Puvion, E. 1995.** p80-coilin: a
14 10 component of coiled bodies and interchromatin granule-associated zones. *J. Cell. Sci.* 108:
15 11 1143-1153.
- 16 12 **Puvion, E., Lange, M. 1980.** Functional significance of perichromatin granule
17 13 accumulation induced by cadmium chloride in isolated rat liver cells. *Experimental Cell*
18 14 *Research* 128: 47-58.
- 19 15 **Raska, I. 1995.** Nuclear ultrastructures associated with the RNA synthesis and processing.
20 16 *J.Cell.Biochem.* 59: 11-26.
- 21 17 **Raska, I., Rychter, Z., Smetana, K. 1983.** Fibrillar centers and condensed nucleolar
22 18 chromatin in resting and stimulated human lymphocytes. *Zeitschrift Fur Mikroskopisch-*
23 19 *Anatomische Forschung* 97: 15-32.
- 24 20 **Raska, I., Koberna, K., Malinsky, J., Fidlerova, H., Masata, M. 2004.** The nucleolus
25 21 and transcription of ribosomal genes. *Biol. Cell* 96: 579-594.
- 26 22 **Raska, I., Andrade, L.E., Ochs, R.L., Chan, E.K., Chang, C.M., Roos, G., Tan, E.M.**
27 23 **1991.** Immunological and ultrastructural studies of the nuclear coiled body with
28 24 autoimmune antibodies. *Experimental Cell Research* 195: 27-37.
- 29 25 **Risueño, M.C., Testillano, P.S. 1994.** Cytochemistry and immunocytochemistry of
30 26 nucleolar chromatin in plants. *MICRON* 25: 331-360.
- 31 27 **Schul, W., Groenhout, B., Koberna, K., Takagaki, Y., Jenny, A., Manders, E.M.,**
32 28 **Raska, I., Van Driel, R., De Jong, L. 1996.** The RNA 3' cleavage factors CstF 64 kDa and
33 29 CPSF 100 kDa are concentrated in nuclear domains closely associated with coiled bodies
34 30 and newly synthesized RNA. *EMBO J.* 15: 2883-2892.
- 35 31 **Seguí-Simarro, J.M., Nuez, F. 2008.** How microspores transform into haploid embryos:
36 32 changes associated with embryogenesis induction and microspore-derived embryogenesis.
37 33 *Physiol. Plant.* 134: 1-12.
- 38 34 **Seguí-Simarro, J.M., Testillano, P.S., Risueño, M.C. 2003.** Hsp70 and Hsp90 change
39 35 their expression and subcellular localization after microspore embryogenesis induction in
40 36 *Brassica napus* L. cv Topas. *J. Struct. Biol.* 142: 379-391.
- 41 37 **Seguí-Simarro, J.M., Testillano, P.S., Risueño, M.C. 2005.** MAP kinases are
42 38 developmentally regulated during stress-induced microspore embryogenesis in *Brassica*
43 39 *napus* L. *Histochem. Cell Biol.* 123: 541-551.
- 44 40 **Seguí-Simarro, J.M., Bárány, I., Suárez, R., Fadón, B., Testillano, P.S., Risueño, M.C.**
45 41 **2006.** Nuclear bodies domain changes with microspore reprogramming to embryogenesis.
46 42 *Eur. J. Histochem.* 50: 35-44.
- 47 43 **Shaw, P.J., Brown, J.W.S. 2004.** Plant nuclear bodies. *Curr. Opin. Plant Biol.* 7: 614-620.
- 48 44 **Spector, D.L. 1993a.** Nuclear organization of pre-mRNA processing. *Curr. Opin. Cell*
49 45 *Biol.* 5: 442-448.
- 50 46 **Spector, D.L. 1993b.** Macromolecular domains within the cell nucleus. *Annu.Rev.Cell*
51 60 *Biol* 9: 265-315.

1
2
3
4
5
6
7
8
9
10
11
12
13
14
15
16
17
18
19
20
21
22
23
24
25
26
27
28
29
30
31
32
33
34
35
36
37
38
39
40
41
42
43
44
45
46
47
48
49
50
51
52
53
54
55
56
57
58
59
60
61
62
63
64
65

1 **Spector, D.L., Schrier, W.H., Busch, H. 1983.** Immunoelectron microscopic localization
2 of snRNPs. *Biol. Cell* 49: 1-10.

3 **Spector, D.L., Fu, X.D., Maniatis, T. 1991.** Associations between distinct pre-mRNA
4 splicing components and the cell nucleus. *EMBO J.* 10-11: 3467-3481.

5 **Supena, E.D.J., Winarto, B., Riksen, T., Dubas, E., van Lammeren, A., Offringa, R.,
6 Boutilier, K., Custers, J. 2008.** Regeneration of zygotic-like microspore-derived embryos
7 suggests an important role for the suspensor in early embryo patterning. *J. Exp. Bot.* 59:
8 803-814.

9 **Testillano, P.S., Coronado, M.J., Seguí-Simarro, J.M., Domenech, J., Gonzalez-
10 Melendi, P., Raska, I., Risueño, M.C. 2000.** Defined nuclear changes accompany the
11 reprogramming of the microspore to embryogenesis. *J. Struct. Biol.* 129: 223-232.

12 **Testillano, P.S., González-Melendi, P., Ahmadian, P., Risueño, M.C. 1995.** The
13 methylation-acetylation (MA) method, an ultrastructural cytochemistry for nucleic acids
14 compatible with immunogold studies. *J. Struct. Biol.* 114: 123-139.

15 **Testillano, P.S., González-Melendi, P., Coronado, M.J., Seguí-Simarro, J.M., Moreno,
16 M.A., Risueño, M.C. 2005.** Differentiating plant cells switched to proliferation remodel
17 the functional organization of nuclear domains. *Cytogenet. Genome Res.* 109: 166-174.

18 **Testillano, P.S., Sánchez-Pina, M.A., Olmedilla, A., Fuchs, J.P., Risueño, M.C. 1993.**
19 Characterization of the interchromatin region as the nuclear domain containing snRNPs in
20 plant cells. A cytochemical and immunoelectron microscopy study. *Eur. J. Cell Biol.* 61:
21 349-361.

22 **Testillano PS, Sanchez-Pina MA, Olmedilla A, Ollacarizqueta MA, Tandler CJ &
23 Risueño MC. 1991.** A specific ultrastructural method to reveal DNA: the NAMA-Ur. *J*
24 *Histochem Cytochem* 39 :1427-1438.

25 **Thiry, M. 1995.** The interchromatin granules. *Histology and Histopathology* 10: 1035-
26 1045.

27 **Vazquez-Nin, G.H., Echeverria, O.M., Ortiz, R., Ubaldo, E., Fakan, S. 1997.** Effects of
28 hypophyseal hormones on transcription and RNA export to the cytoplasm. *Experimental*
29 *Cell Research* 236: 519-526.

30 **Visa, N., Puvion-Dutilleul, F., Bachellerie, J.P., Puvion, E. 1993.** Intranuclear
31 distribution of U1 and U2 snRNAs visualized by high resolution in situ hybridization:
32 revelation of a novel compartment containing U1 but not U2 snRNA in HeLa cells. *Eur. J.*
33 *Cell Biol.* 60: 308-321.

34 **Williams, M. 1977.** Stereological techniques. In *Practical methods in electron microscopy*,
35 ed. by A.M. Glauert North Holland/American Elsevier. Amsterdam:

38

1
2
3
4 **Figure legends**
5
6
7

8 **Figure 1: Early stages of microspore embryogenesis.** A: Freshly isolated
9
10 microspores and young bicellular pollen. B: Induced microspores. C: Early (octant) MDE.
11
12 D: Globular MDE. E: Heart-shaped MDE. Insets in figures A-D are sections of microspores
13
14 and MDEs at the corresponding stages. Bars in A, B: 10 μ m. C-E: 50 μ m.
15
16
17
18
19

20 **Figure 2: Overview of the nuclear architecture during microspore**
21
22 **embryogenesis:** Vacuolate microspore (A) and heart-shaped MDE nuclei (B) in MA-
23
24 treated sections. Note the remarkably different organization of the different components of
25
26 the interchromatic region (ir) in both cell types. cb: Cajal body; chr: condensed chromatin;
27
28 dfc: nucleolar dense fibrillar component; ex: exine coat; fc: nucleolar fibrillar center; gc:
29
30 nucleolar granular component; ne: nuclear envelope; nu: nucleolus; nv: nucleolar vacuole;
31
32 v: vacuole. Bars: 500 nm.
33
34
35
36
37
38
39

40 **Figure 3: Changes in nuclear architecture during pollen maturation.** The A, B
41
42 and C series of figures cover the changes in nuclear organization undergone by young
43
44 bicellular pollen, mid bicellular pollen and mature, tricellular pollen respectively. The
45
46 A'B'C' and A''B'' columns show the IR of the vegetative and generative nucleus
47
48 respectively. C'' correspond to a sperm nucleus of tricellular pollen. All figures but C are
49
50 respectively. C'' correspond to a sperm nucleus of tricellular pollen. All figures but C are
51
52 from EDTA-treated sections. See text for further details. Bars in A-C: 5 μ m. A'-C'': 500
53
54 nm.
55
56

57 **Figure 4: Morphometric analysis of nuclear size.** Estimation by the average
58
59 nuclear area during microspore embryogenesis (A) and pollen maturation (B). Bars
60
61
62
63
64
65

1 represent the average nuclear area over TEM micrographs measured in μm^2 . Mic: isolated
2 microspores; Ind: induced microspores; EG: early globular MDE; LG: late globular MDE;
3 HS: heart-shaped MDE; Nv: vegetative nucleus; Ng: generative nucleus. See text for
4 further details.

5
6 **Figure 5: The condensed chromatin and the perichromatin region after**
7 **cytochemical techniques for nucleic acids (MA), RNPs (EDTA) and DNA (NAMA-Ur)**
8 **in globular MDEs.** Nuclear regions showing a chromatin mass. A: MA staining for nucleic
9 acids; condensed chromatin (chr) displays higher contrast than the nucleolus (nu) and
10 interchromatin RNP structures. B: EDTA staining for RNPs; condensed chromatin (chr)
11 appears bleached whereas the nucleolus (nu) and RNP fibers and granules of the IR show
12 contrast. C: NAMA-Ur staining for DNA; only condensed chromatin masses (chr) and
13 chromatin fibres at the perichromatin region (arrows) and in the IR show high contrast,
14 whereas the nucleolus (nu) and cytoplasm (ct) show no contrast at all. Bars: 300 nm.

15
16 **Figure 6: The interchromatin region in EDTA-treated sections of globular**
17 **MDE cells.** A: nuclear overview showing the nucleolus (nu), the bleached chromatin
18 masses (chr) and the interchromatin region (ir). B, C: magnifications of the regions boxed
19 in A. Arrowheads in B: perichromatin fibrils. Dotted line in C: interchromatin granule-
20 associated zone. D: interchromatin region with perichromatin granules. E: magnification of
21 the area boxed in D. Arrows point to perichromatin granules. ne: nuclear envelope. Bars in
22 A: 500 nm. B-E: 200 nm.

1
2
3
4 1 **Figure 7: Anti-TMG immunofluorescence over cryosections during**
5
6 2 **gametophytic and embryogenic development.** A-E: DAPI staining. A'-E': anti-TMG.
7
8 3 Yellow arrowheads point to CBs. Note the absence of DNA in the corresponding regions in
9
10 4 DAPI-stained images (compare white arrows in A and A'). The asterisk in A marks the
11
12 5 massive vacuole of the microspore. Bars: 10 μm .
13
14
15
16
17
18

19 7 **Figure 8: Anti-TMG immunogold labelling in microspores and MDEs.** A:
20
21 8 interchromatin region (ir) of a vacuolate microspore showing an intensely labelled Cajal
22
23 9 body (cb). B: Interchromatin region of an early globular MDE showing abundant labelling
24
25 10 over one electron-light (centrally located) and two electron-dense CBs (at both sides). C:
26
27 11 Overview of the interchromatin region of a heart-shaped MDE, showing a large, round and
28
29 12 circular CB between the nucleolus (nu) and a mass of condensed chromatin (chr). Arrows
30
31 13 indicate clusters of gold particles over the IR, whereas arrowheads point to particles
32
33 14 decorating the borders of chromatin masses. D-E: EDTA-treated sections where CB-
34
35 15 marking gold particles concentrate into small clusters on the IR (arrows), over a EDTA-
36
37 16 positive (RNP-containing) CB (outlined in D), and also over a CB-associated zone (cb-az).
38
39 17 ct: cytoplasm; ex: exine coat; ne: nuclear envelope. Bars: 200 nm.
40
41
42
43
44
45
46
47

48 19 **Figure 9: Quantitative analysis of Cajal bodies during microspore**
49
50 20 **embryogenesis.** A: mean CB number per nuclear μm^2 . B: mean individual CB area per
51
52 21 nuclear μm^2 . C: mean total CB area per nuclear μm^2 . D: Frequency distribution, expressed
53
54 22 in percentage, of the areas of the different CBs observed. See text for further details. E:
55
56 23 example of a large, electron light CB. F: example of small, electron dense CB. Mic:
57
58
59
60
61
62
63
64
65

1
2
3
4
5
6
7
8
9
10
11
12
13
14
15
16
17
18
19
20
21
22
23
24
25
26
27
28
29
30
31
32
33
34
35
36
37
38
39
40
41
42
43
44
45
46
47
48
49
50
51
52
53
54
55
56
57
58
59
60
61
62
63
64
65

1 isolated microspores; Ind: induced microspores; EG: early globular MDE; LG: late globular
2 MDE; HS: heart-shaped MDE. Bars: 200 nm.

3

4 **Figure 10: Summary of the changes in the chromatin condensation and IR**
5 **structures in both pollen programs: pollen development (differentiation process) and**
6 **microspore embryogenesis (proliferation process).** IGs: Interchromatin granules, CBs:
7 Cajal bodies. – : absence, +/-: low amount, +: present, ++: abundant, +++: high abundant.

Figure 1
[Click here to download high resolution image](#)



Figure 2
[Click here to download high resolution image](#)

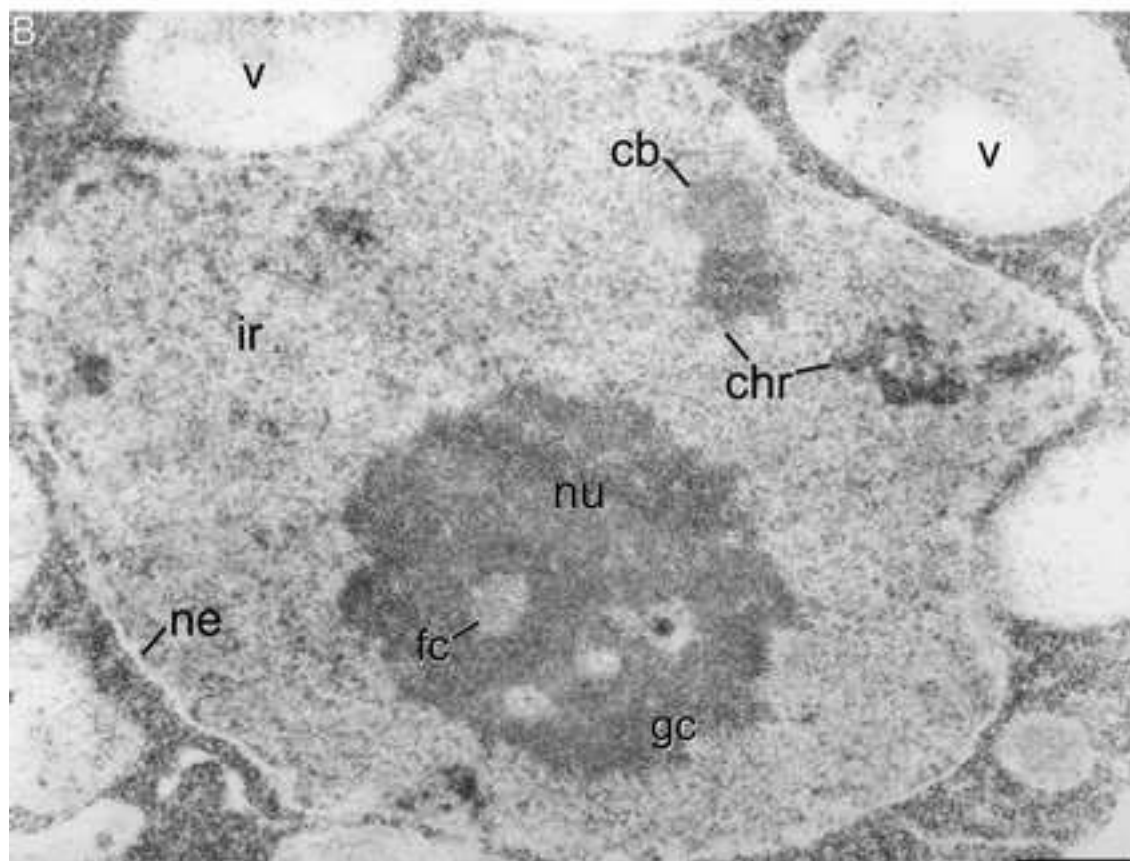
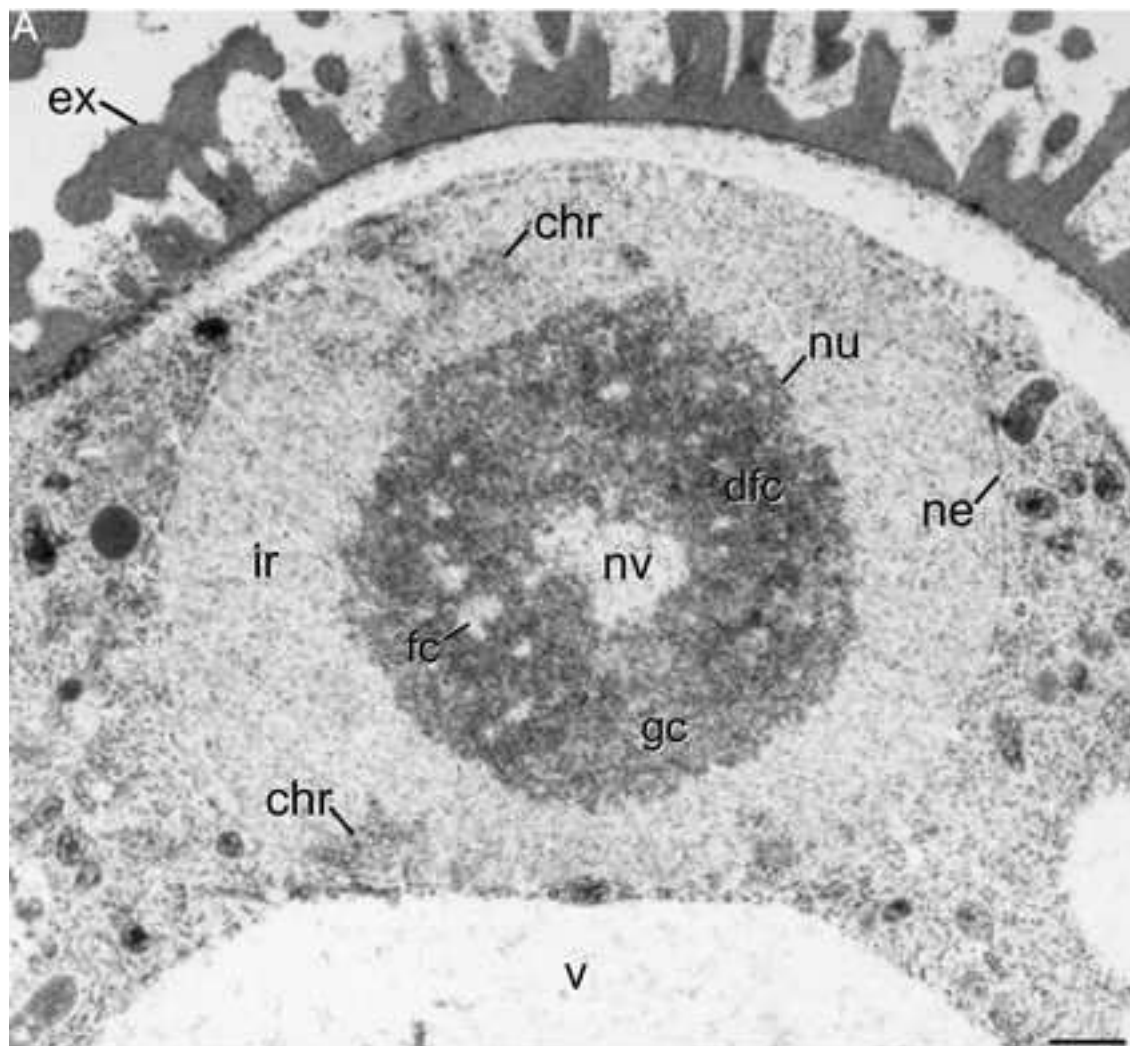


Figure 3
[Click here to download high resolution image](#)

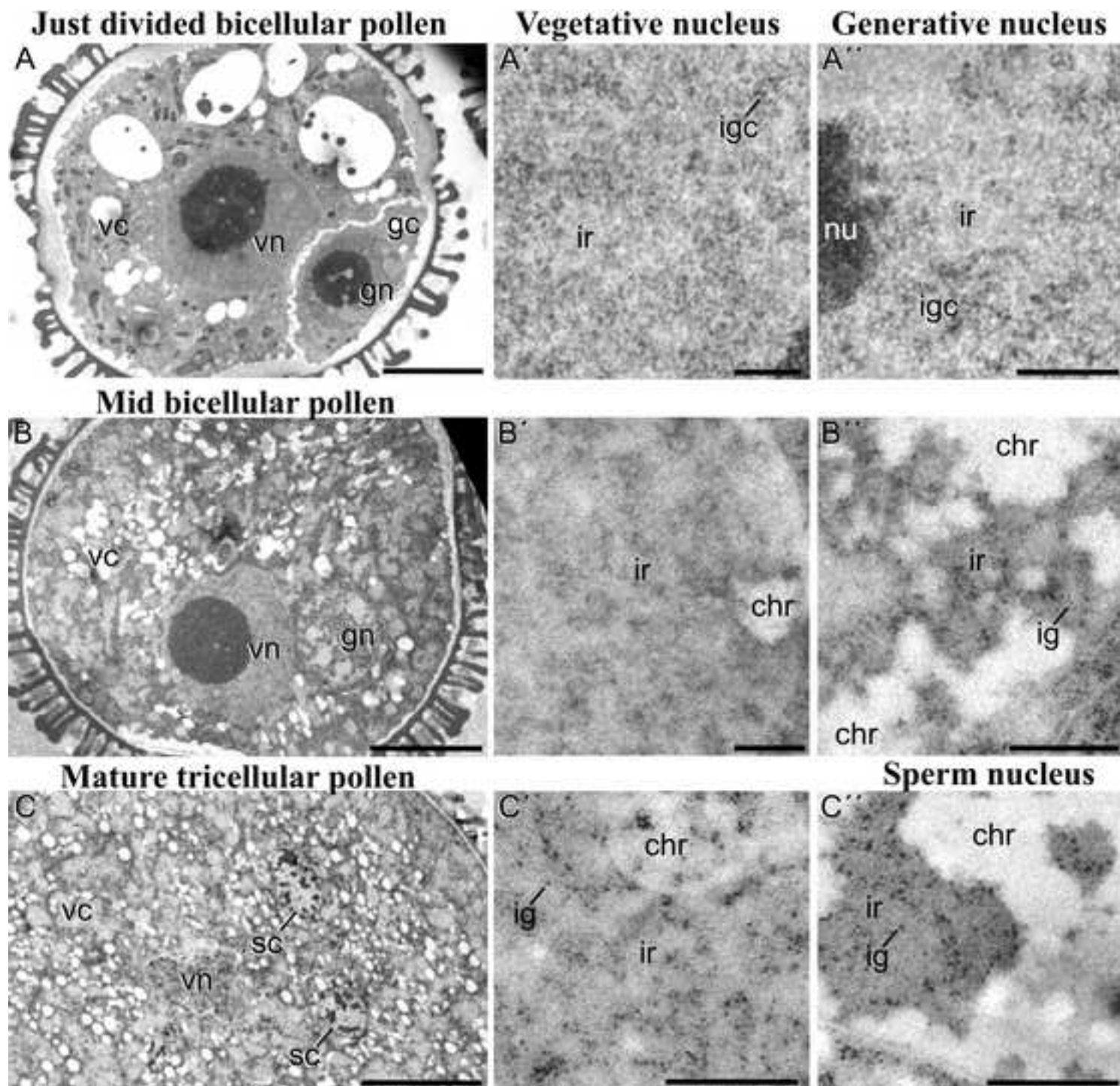


Figure 4
[Click here to download high resolution image](#)

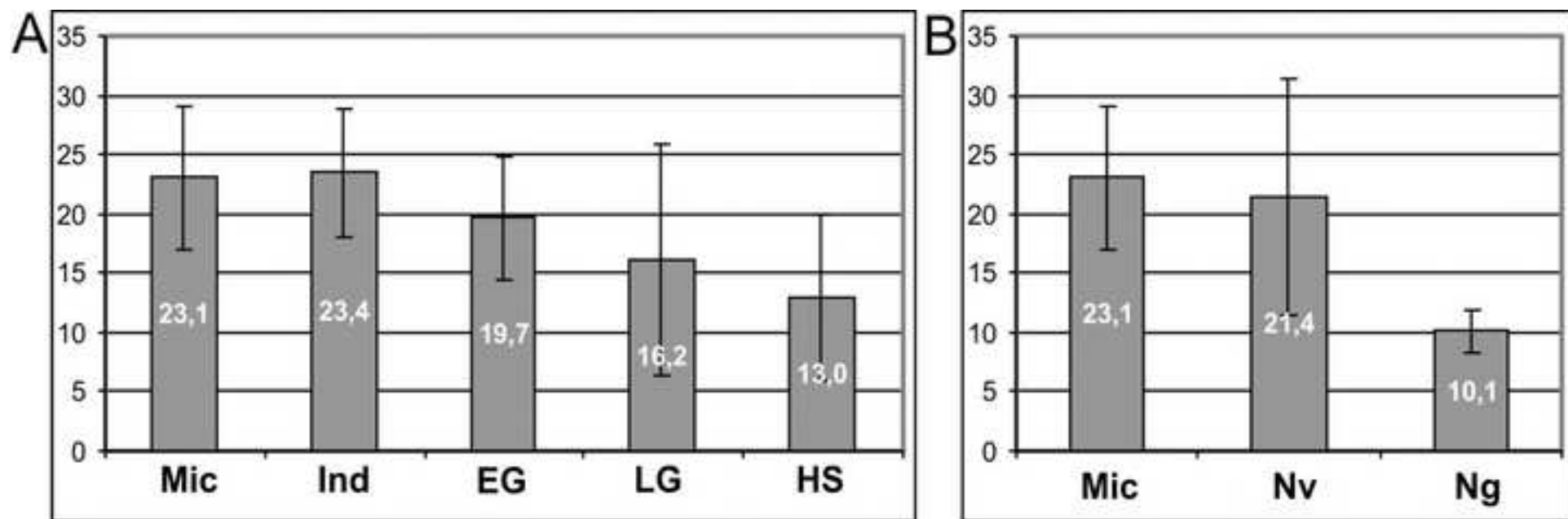


Figure 5

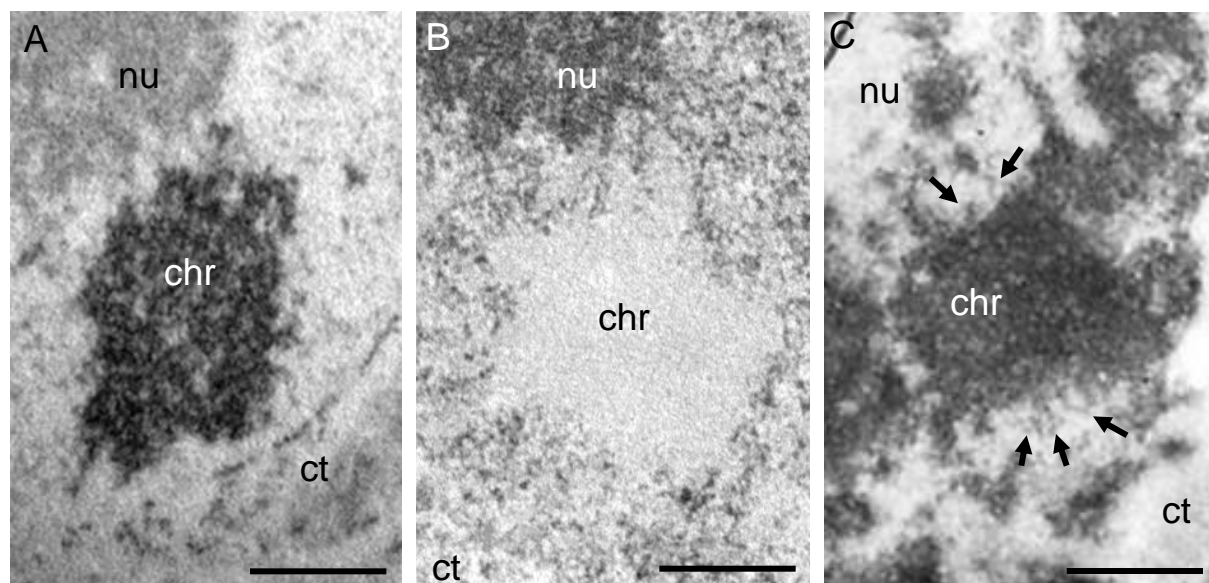


Figure 5

Figure 6
[Click here to download high resolution image](#)

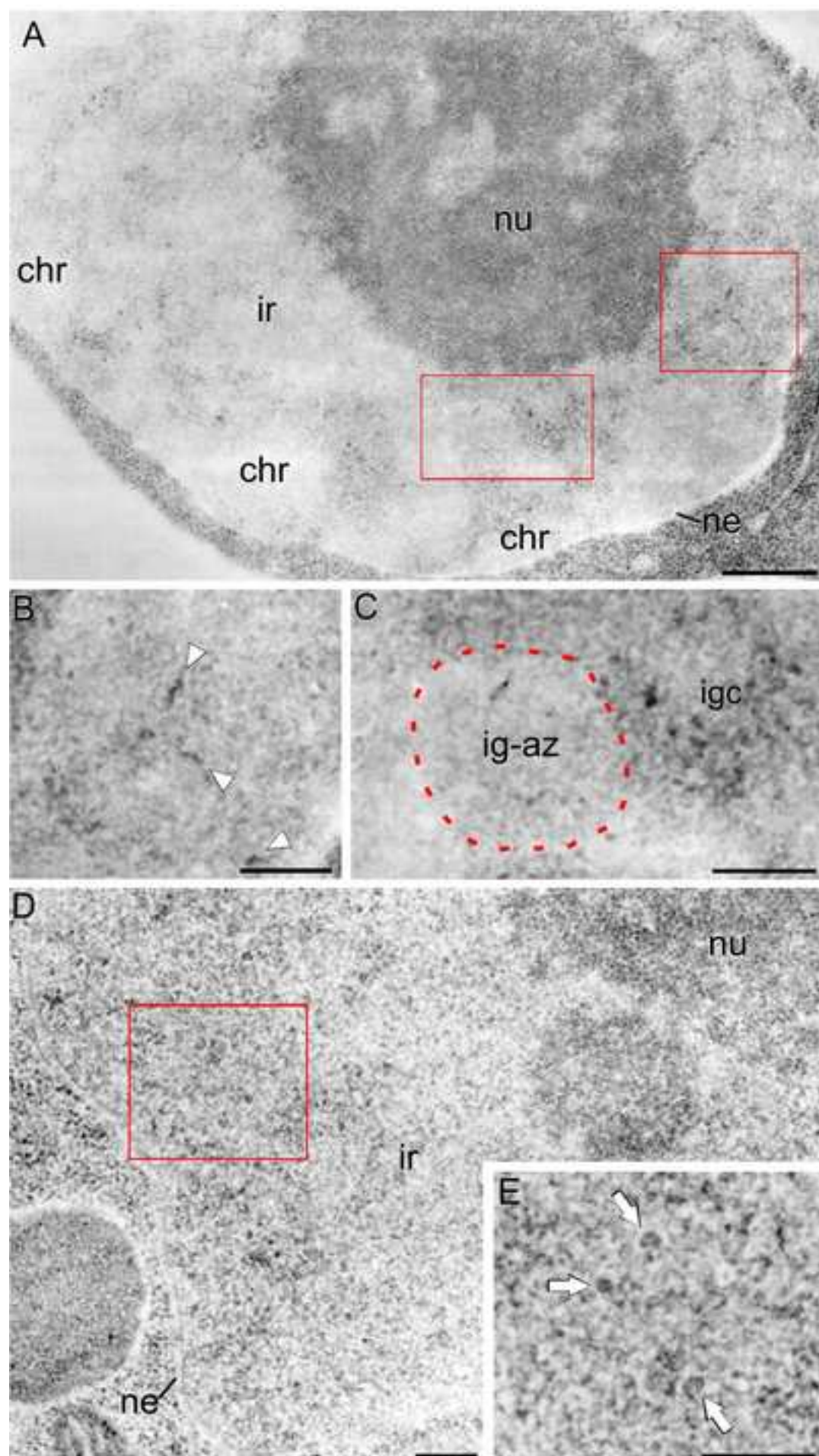


Figure 7
[Click here to download high resolution image](#)

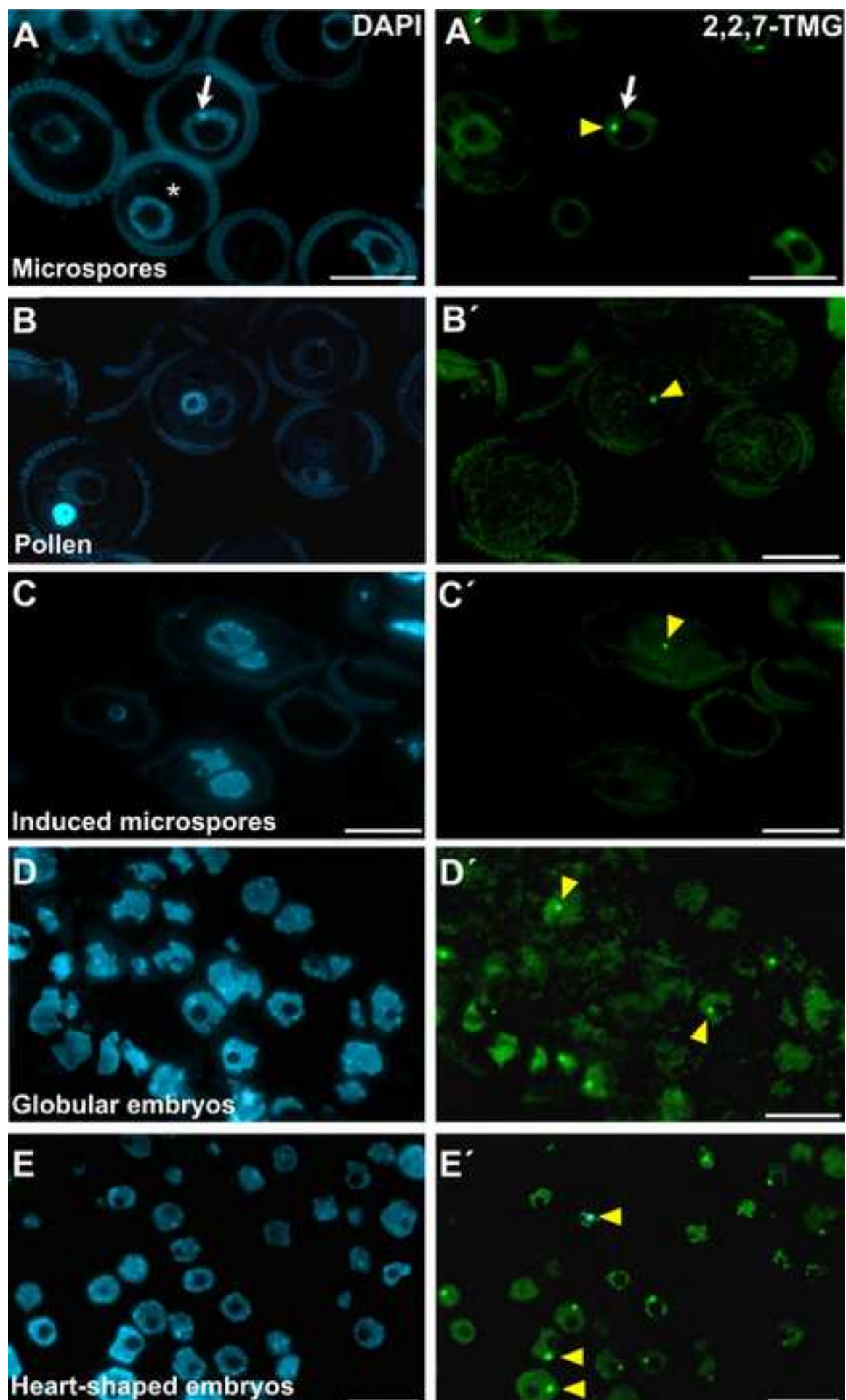


Figure 8
[Click here to download high resolution image](#)

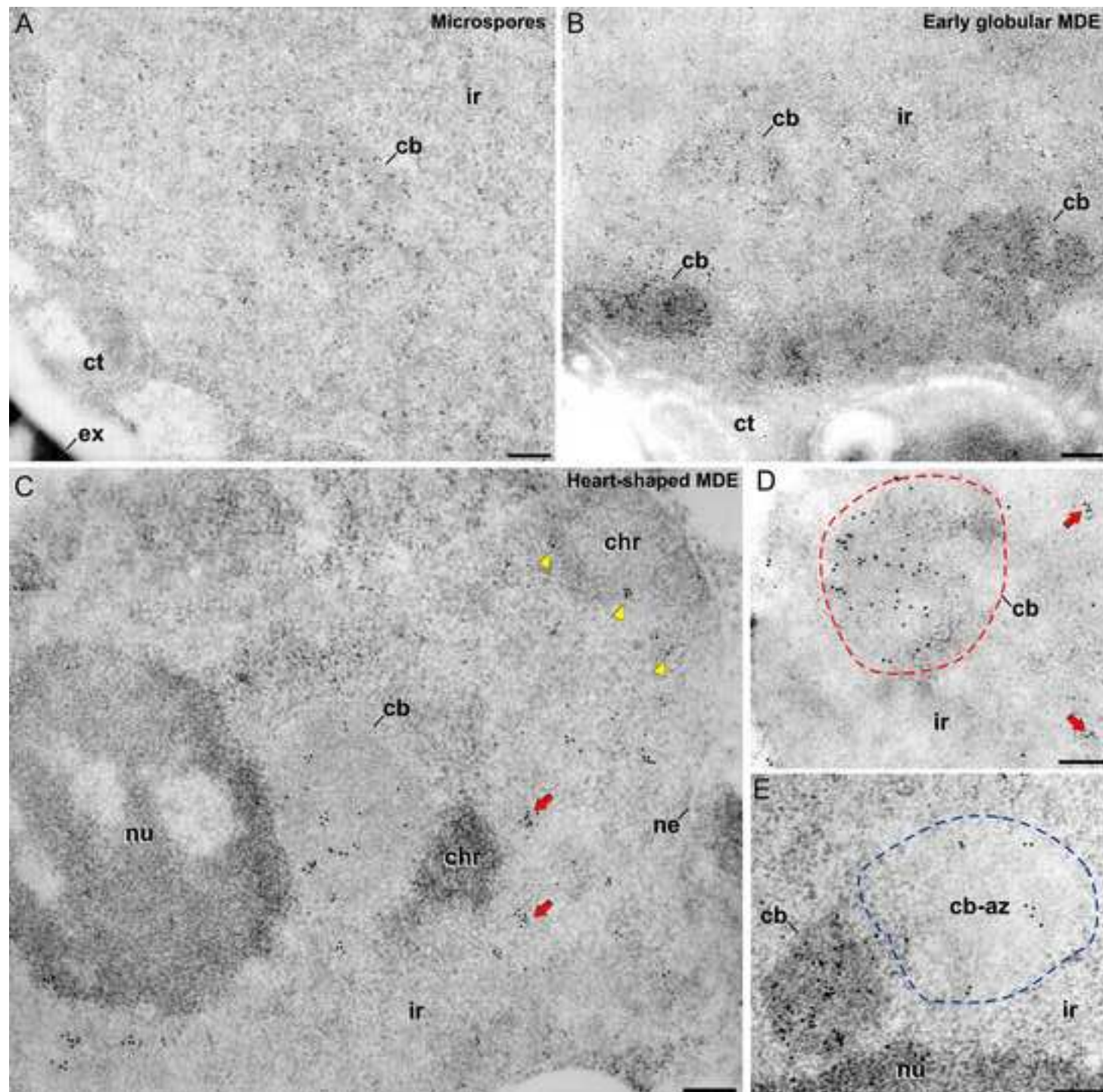


Figure 9

[Click here to download high resolution image](#)

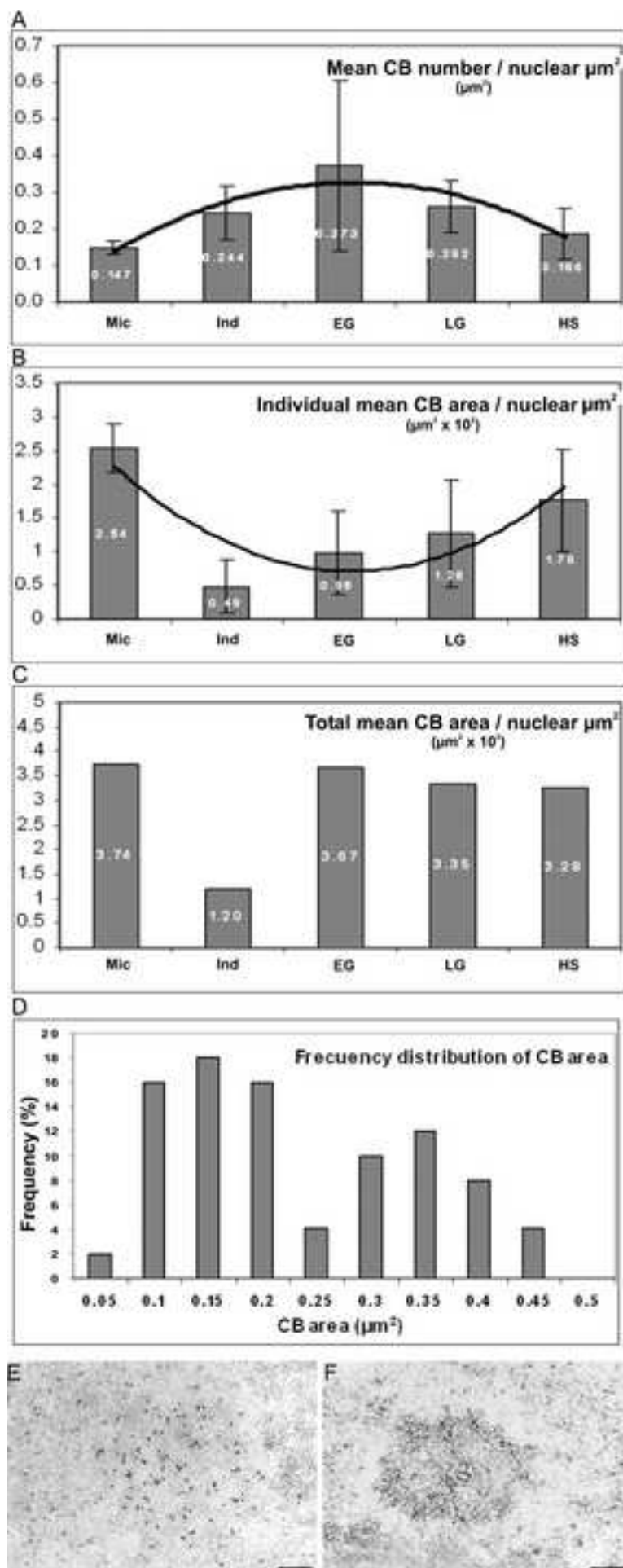


Figure 10



		DIFFERENTIATION  Pollen development			PROLIFERATION  Microspore embryogenesis		
		Young pollen	Mid pollen	Mature pollen	Vacuolate microspore	Multicellular microspore	Microspore derived embryo MDE
Chromatin condensation		+/-	++	+++	+/-	+/-	+/-
IR structures	Isolat. IGs	+	++	+++	+	+	+
	IG clusters	++	+	-	+++	++	++
	CBs	+	+/-	-	+	++	+++

Figure 10